ADVANCED FUNCTIONAL MATERIALS
www.afm-journal.de

# Isopropanol: A Green Solvent Additive for 20% Efficiency Organic Solar Cells with Excellent Generality and Improved Eco-Compatibility

*Bing Guo, Jiaqi Li, Kai Xiang, Jinyuan Zhang, Shuhui Ding, Wendi Shi, Tengfei Li, Hairui Bai, Qunping Fan, Zhaoyang Yao,* Xiangjian Wan, Yongfang Li, and Yongsheng Chen**

**Solvent additive engineering has been regarded as the most common and effective approach to finely tune the bulk heterojunction (BHJ) morphology of organic solar cells (OSCs). However, most conventional solvent additives are environmentally unfriendly and difficult to completely remove due to their toxicity and high boiling points. Herein, isopropanol (IPA) is first reported as a green solvent additive to significantly improve the photovoltaic performance of OSCs. Notably, the addition of IPA can facilitate the formation of highly ordered molecular stacking and suppress charge recombination in OSCs through precisely modulating molecular aggregation behaviors during film formation. As a result, the IPA processed PM6:BTP-eC9-based OSC yields an impressive power conversion efficiency (PCE) of 20.0%, which is much higher than 18.2% for that without additives. Furthermore, the all-green-solvent processed OSCs based on PM6:BTP-eC9-4ClO with o-xylene as the main solvent and IPA as an additive achieve a high PCE of 19.4%. With the combined high device efficiency, excellent generality and improved eco-compatibility, the morphology control strategy with IPA as an additive provides a new promising route toward commercial OSC technology.**

## 1. Introduction

Organic solar cells (OSCs) have attracted significant attention due to their advantages of solution processability, mechanical flexibility, and potential for low-cost, large-area fabrication.[1,2] Remarkable progress has contributed to power conversion efficiencies (PCEs) now exceeding 20%.[3–15] Despite these advances, the overall performance of OSCs remains fundamentally constrained by non-ideal exciton and free charge carrier transport, which not only relies on the intrinsic molecular structures of the organic donor/acceptor materials, but also needs suitable morphology within the bulk heterojunction (BHJ) active layer.[16–18] Achieving an optimal blend morphology is important, as it not only facilitates efficient exciton dissociation, but also promotes balanced carrier transport and suppresses unexpected recombination pathways, thereby enhancing the overall photovoltaic performance.[19]

Many strategies have been developed to finely tune the BHJ morphology of the active layer, primarily through additive-mediated strategy, thermal annealing, and solvent vapor annealing.[20] Among these, additive engineering has emerged as the most common and effective approach for fine-tuning molecular packing and phase separation.[21] However, most conventional additives currently utilized-encompassing both liquid (e.g., 1,8-diiodooctane) and

B. Guo, J. Li, S. Ding, W. Shi, Z. Yao, X. Wan, Y. Chen
State Key Laboratory and Institute of Elemento-Organic Chemistry
Frontiers Science Center for New Organic Matter
Nanoscale Science and Technology and Key Laboratory of Functional Polymer Materials
Renewable Energy Conversion and Storage Center (RECAST)
College of Chemistry
Nankai University
Tianjin 300071, China
E-mail: zyao@nankai.edu.cn; yschen99@nankai.edu.cn

K. Xiang, T. Li, H. Bai, Q. Fan
State Key Laboratory for Mechanical Behavior of Materials
Xi'an Jiaotong University
Xi'an 710049, China

J. Zhang, Y. Li
CAS Key Laboratory of Organic Solids
Institute of Chemistry
Chinese Academy of Sciences
Beijing 100049, China

Y. Li
Laboratory of Advanced Optoelectronic Materials
College of Chemistry
Chemical Engineering and Materials Science
Soochow University
Suzhou 215123, China

The ORCID identification number(s) for the author(s) of this article can be found under https://doi.org/10.1002/adfm.202518732

**DOI: 10.1002/adfm.202518732**

 

solid types (e.g., halogenated thiophenes)-usually contain halogen atoms.[22] This raises significant environmental concerns and conflicts with the pursuit of sustainable organic electronics. Furthermore, commonly used solvent additives with high boiling points are challenging to be removed completely during post-processing, which is harmful to both device stability and long-term operational durability.[23] Therefore, the development of novel and green solvent additives is urgently needed to achieve simultaneously high performance, excellent generality, and improved eco-compatibility in OSCs.

In this study, for the first time, we report a morphology control strategy with alcohol as solvent additives to finely tune the BHJ morphology and significantly improve the device performance of OSCs. The addition of three alcohols, including methanol (MeOH), ethanol (EtOH), and isopropanol (IPA) can precisely modulate the molecular aggregation during film formation, which facilitates the formation of highly ordered molecular stacking and high-quality fibril-like bicontinuous network morphology. This suppresses charge recombination and facilitates charge transport in the devices. As a result, the IPA processed PM6:BTP-eC9-based device yielded an impressive efficiency of 20.0%, with an open-circuit voltage ($V_{oc}$) of 0.856 V, a high short-circuit current density ($J_{sc}$) of 28.89 mA cm$^{-2}$, and a fill factor (FF) of 80.9%, which is much higher than the device without additive (PCE of 18.2%). Furthermore, the all-green-solvent processed OSCs based on PM6:BTP-eC9-4ClO with o-xylene as the main solvent and IPA as an additive gave a high PCE of 19.4%. With the combined high device efficiency, excellent generality, and improved eco-compatibility, the morphology control strategy with IPA as an additive provides a new promising route toward commercial OSC technology.

## 2. Results and Discussion

### 2.1. Materials and Device Performance

The chemical structures of the conjugated polymer donor PM6, small molecule acceptor (SMA) BTP-eC9, and three alcohol-based solvent additives (i.e., MeOH, EtOH, and IPA) are shown in **Figure 1**a,b. The absorption spectra of pure films and blend films processed with different solvent additives are presented in Figure 1c–e. PM6 primarily absorbs short-wavelength photons between 500 and 700 nm, while BTP-eC9 mainly absorbs light from 600 to 900 nm, which shows complementary absorption with that of PM6. The incorporation of alcohols into PM6 films reduces the 0–1 vibronic transition intensity ($I_{0\text{-}1}$) and leads to a higher ratio of $I_{0\text{-}0}/I_{0\text{-}1}$, suggesting an enhanced ordered *J*-aggregation behaviour.[24] Meanwhile, alcohol-treated PM6 films show slightly red-shifted absorption spectra compared to the pristine PM6 film without additives. Particularly, the IPA-treated PM6 film exhibits a higher ratio of $I_{0\text{-}0}/I_{0\text{-}1}$ and more red-shifted absorption characteristic, which indicates that IPA could induce more ordered interchain stacking than the other alcohols.[25] As for the BTP-eC9 films processed with different additives, decreased 0–1 vibronic transition intensities are also observed relative to the control BTP-eC9 film, which indicates that the addition of alcohol as additives can also promote the molecular packing of BTP-eC9. Furthermore, the absorption coefficient of pure films and especially the blend films is significantly enhanced with alcohol as additives (Figure 1e; Figure S1, Supporting Information), which may enhance the light utilization within the absorption region.

**Table 1.** Photovoltaic parameters of the OSCs with different solvent additives under the illumination of AM 1.5 G, 100 mW cm$^{-2}$.

| Additive | $V_{oc}$ [V] | $J_{sc}$ [mA cm$^{-2}$] | FF [%] | PCE[a] [%] |
|---|---|---|---|---|
| w/o | 0.852 | 27.38 | 78.1 | 18.2 (18.1 ± 0.12) |
| MeOH | 0.850 | 28.10 | 79.7 | 19.0 (19.0 ± 0.07) |
| EtOH | 0.853 | 28.63 | 80.0 | 19.5 (19.4 ± 0.12) |
| IPA | 0.856 | 28.89 | 80.9 | 20.0 (19.8 ± 0.13) |

[a] The average values and standard deviations were obtained from statistical analysis of 10 individual devices.

Solar cell devices were fabricated with a conventional structure of Glass/ITO/2PACz/PM6:BTP-eC9/PNDIT-F3N/Ag. The ratios of three alcohol-based solvent additives have been scanned from 0.5% to 1.5% by volume, and the optimal ratio is 1% (Figure S2 and Table S1, Supporting Information). The current density-voltage (*J-V*) curves of OSC devices processed with different additives (1% by volume) are depicted in Figure 1f, and the corresponding photovoltaic parameters are summarized in **Table 1**. The device processed without additives exhibits a maximum PCE of 18.2%, with a $V_{oc}$ of 0.852 V, a $J_{sc}$ of 27.38 mA cm$^{-2}$, and a FF of 78.1%. When adding alcohol as additives, the device performances are enhanced gradually from MeOH to IPA (Figure 1h). Surprisingly, for the IPA based devices, a highest PCE of 20.0% is obtained with a $V_{oc}$ of 0.856 V, an enhanced $J_{sc}$ of 28.89 mA cm$^{-2}$, and a high FF of 80.9%. The slightly enhanced $V_{oc}$ is attributed to the low energy loss ($E_{loss}$) of 0.540 eV in OSCs processed with IPA as an additive (Figures S3, S4a, and Table S2, Supporting Information). Reduced Urbach energy contributes to decreasing the $E_{loss}$, which suggests a lower energetic disorder for IPA-based device (Figure S4b, Supporting Information). Notably, the achieved efficiency of 20.0% represents one of the highest reported values for PM6:BTP-eC9-based binary systems to date. Furthermore, apart from the storage stability, both the thermal and photo-stability are enhanced for the devices processed with IPA as an additive (Figures S5 and S6, Supporting Information). External quantum efficiency (EQE) results show an increase in EQE response for the alcohol processed devices, and the device with IPA shows the highest values (Figure 1g). The integrated current from the EQE data of the devices without and with MeOH, EtOH, and IPA as additives are 26.29, 27.20, 27.31, and 27.56 mA cm$^{-2}$, respectively, which are consistent with the $J_{sc}$ derived from the *J-V* curves.

### 2.2. Device Physics Analysis

To investigate the influence of alcohol on the device performances, the exciton dissociation ($P_{diss}$) and charge collection ($P_{coll}$) efficiency of these devices were first investigated from the dependence of photocurrent density ($J_{ph}$) on the effective voltage ($V_{eff}$). As shown in **Figure 2**a and Table S3 (Supporting Information), the IPA based device exhibits the highest $P_{diss}$ (98.38%) and $P_{coll}$ (93.54%) values, higher than the devices without and with MeOH and EtOH as additives, which means a higher capability

 

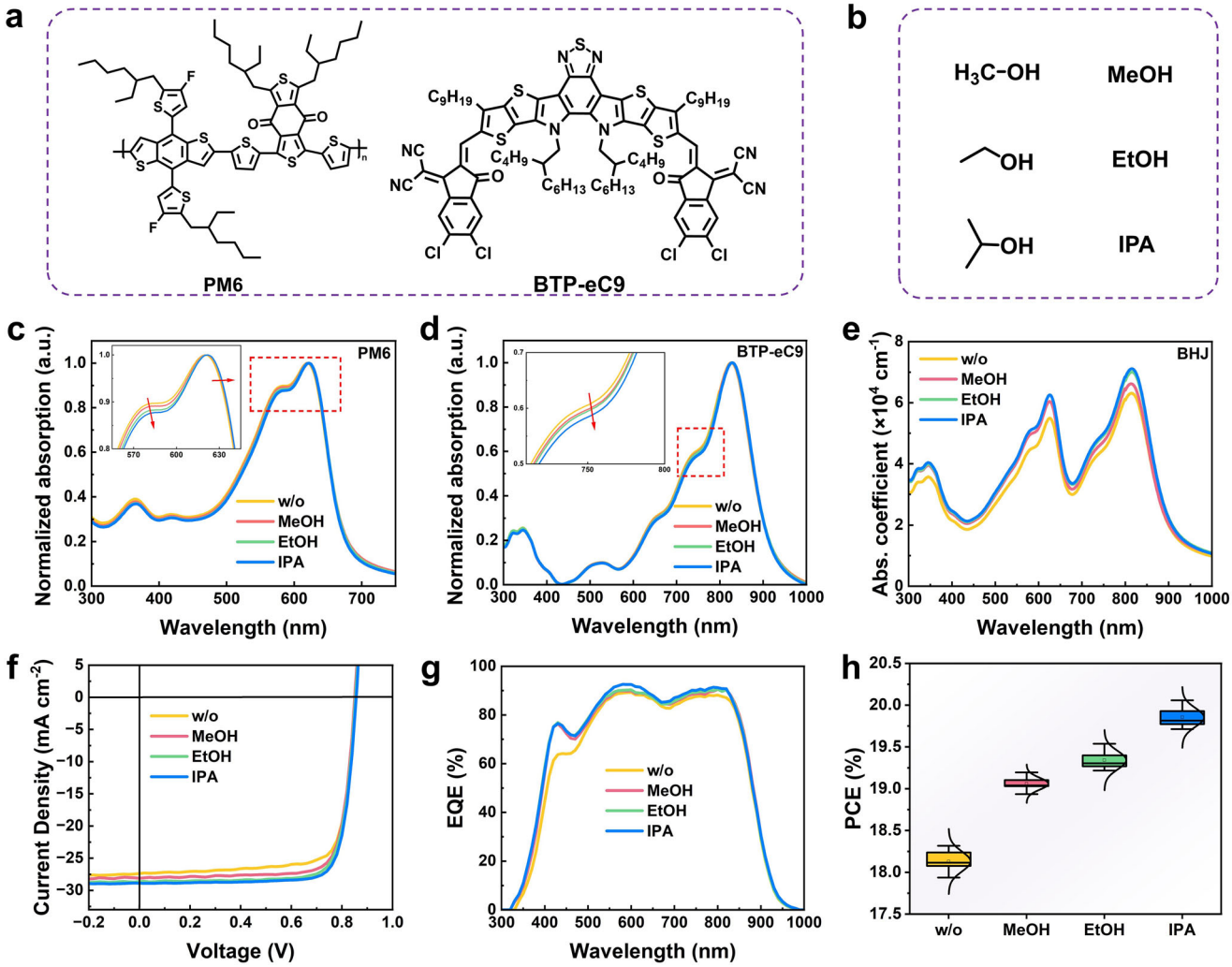


**Figure 1.** a) Molecular structures of PM6 a BTP-eC9, and b) solvent additives. Absorption spectra of c) PM6, d) BTP-eC9, and e) PM6:BTP-eC9 blend films processed with different solvent additives. f) *J-V*, g) EQE curves, and h) statistics of PCE of OSC devices processed with different solvent additives.

in exciton dissociation and charge collection for the device with IPA as an additive. To investigate the carrier transport properties of the devices, space charge limited current (SCLC) measurements were performed.[26] As shown in Figure 2b, Figure S7, and Table S4 (Supporting Information), alcohol-processed devices exhibit enhanced and more balanced hole/electron mobilities, with the IPA based devices demonstrating the highest mobility of 6.87 $\times 10^{-4}$ and 9.21 $\times 10^{-4}$ $cm^2$ $V^{-1}$ $s^{-1}$ for hole and electron, respectively. The enhanced and well-balanced charge carrier mobility in IPA-processed devices can promote efficient charge transport and reduce charge recombination loss, yielding superior $J_{sc}$ and FF.

An efficient charge transport with negligible recombination loss is important for achieving an ideal FF. Considering the high FF in IPA based devices, the degree of bimolecular and trap assisted recombination of these devices were studied through the formula: $J_{sc} \propto \alpha P_{light}$ and $V_{oc} \propto n \ln P_{light}$.[27] As depicted in Figure 2c and Figure S8 (Supporting Information), IPA based devices exhibit the smallest n value (1.15 KT $q^{-1}$) and highest $\alpha$ value (0.997), demonstrating suppressed bimolecular and trap assisted recombination in the IPA-processed devices.

Furthermore, the transient photovoltage (TPV) measurements were also conducted to investigate the charge carrier lifetime and charge recombination. The values of charge carrier lifetime are 49.9, 93.7, 96.7, and 120.3 µs for the OSC devices without and with MeOH, EtOH, and IPA as additives, respectively (Figure 2d). The longer carrier lifetime in IPA-based device indicates efficient suppression of charge carrier recombination, which contributes to a higher FF. Transient photocurrent (TPC) measurements were performed to investigate the charge extraction capability in the devices.[28] As shown in Figure 2e, the charge extraction times are 0.46, 0.38, 0.38, and 0.34 µs for the devices without and with additives of MeOH, EtOH, and IPA, indicating the enhanced charge extraction ability in the devices with IPA as an additive.

To gain more insights into the exciton dissociation and recombination dynamics in the devices, transient absorption (TA) spectroscopy measurements were conducted.[29,30] An excitation wavelength of 800 nm was chosen to selectively excite the SMA

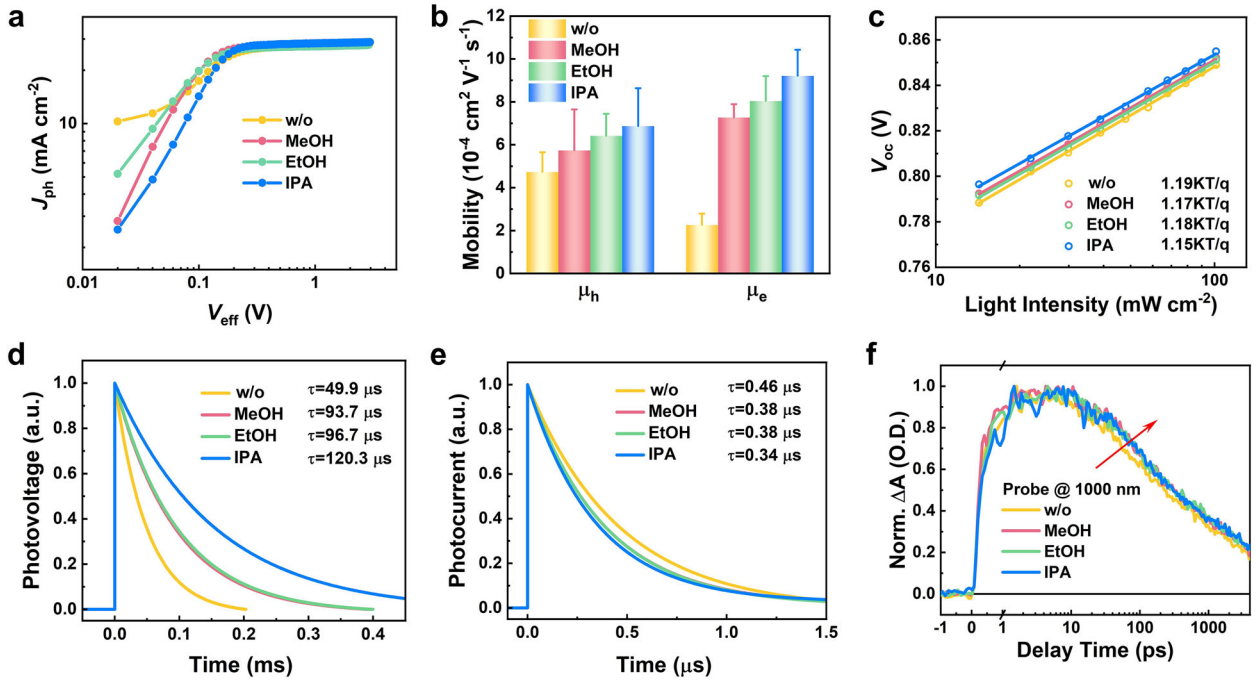


**Figure 2.** a) $J_{ph}$ versus $V_{eff}$ curves of the OSCs. b) Charge carrier mobilities of the OSCs. c) The dependence of $V_{oc}$ on the light intensity of the OSCs. d) TPV and e) TPC curves of the OSCs. f) kinetic traces of CT state ESA probing at 1000 nm for the blend films.

BTP-eC9. Time-resolved 2D TA spectra for the blends with different additives and the corresponding TA profiles at different delay times are illustrated in Figure S9 (Supporting Information). The TA spectra for all the blend films show two distinct ground-state bleach (GSB) peaks at 730 and 850 nm, and excited-state absorption (ESA) signal at 920 nm, which belongs to the excited state of the SMA BTP-eC9. The peaks at 580 and 630 nm correspond to the GSB of the polymer donor PM6, arising from the ultrafast hole transfer from BTP-eC9 to PM6. The rapid attenuation for the GSB and ESA peaks of the SMA indicates the occurrence of charge transfer (CT) between PM6 and BTP-eC9. Figure S10 (Supporting Information) and Figure 2f show the kinetic traces of the CT state with the GSB peak for PM6 at 636 nm and the ESA peak for BTP-eC9 at 1000 nm, respectively. The kinetic curves of the blend films for the GSB signal of the donor exhibit no obvious change. While for the ESA signal of the acceptor, the decays of the films with alcohol as additives are slower than that without additives (Figure 2f), indicating a lower recombination rate, which corresponds to the enhanced FF for the devices with additives.

### 2.3. Morphology

In situ UV–vis absorption measurements were conducted to explore the effect of alcohols on the film formation dynamics. As shown in **Figures** 3a and Figure S11 (Supporting Information), the film formation process of the blend films can be divided into three stages during the spin coating process, i) solvent evaporation, ii) nucleation/crystal growth, and iii) completion of crystal growth. In the first stage, the peak intensity of the donor and acceptor distinctly decreases when the solvent evaporates, while the absorption peak remains unchanged. During the second stage, the absorption peaks exhibit a rapid redshift, especially for the SMA BTP-eC9, due to increased molecular aggregation. Then the peak positions remain unchanged, indicating the completion of crystal growth. As depicted in Figure 3b, the crystallization times are 200, 190, 160, and 150 ms for the blend films without and with MeOH, EtOH, and IPA as additives, respectively. This demonstrates that the addition of alcohols, as poor solvents for the active layer materials, could facilitate the crystallization of both PM6 and BTP-eC9. The decreased crystallization time could suppress the over-aggregation of the active layer materials and reduce undesired charge recombination.

Apart from the spin coating process, the in situ absorption of PM6:BTP-eC9-based films during thermal annealing were also measured. As shown in Figure S12 (Supporting Information), the absorption spectra exhibit negligible changes, indicating that the alcohol additives have no obvious impact on the annealing process of the active layer. Furthermore, the vertical distribution of the blend films was investigated by employing film depth-dependent light absorption spectroscopy (FLAS) (Figure S13, Supporting Information).[31] As exhibited in Figure 3c, Figure S14, and Table S5 (Supporting Information), after adding alcohol as solvent additives, these films show relatively more balanced vertical phase distribution between PM6 and BTP-eC9 throughout the entire active layers, which can also reduce recombination during the carrier transport process.

To investigate the morphology of the blend films with different additives, atomic force microscopy (AFM) and transmission electron microscopy (TEM) were conducted. As shown in **Figures** 4a and S15 (Supporting Information), an obvious phase separation and interpenetrating network can be seen in all

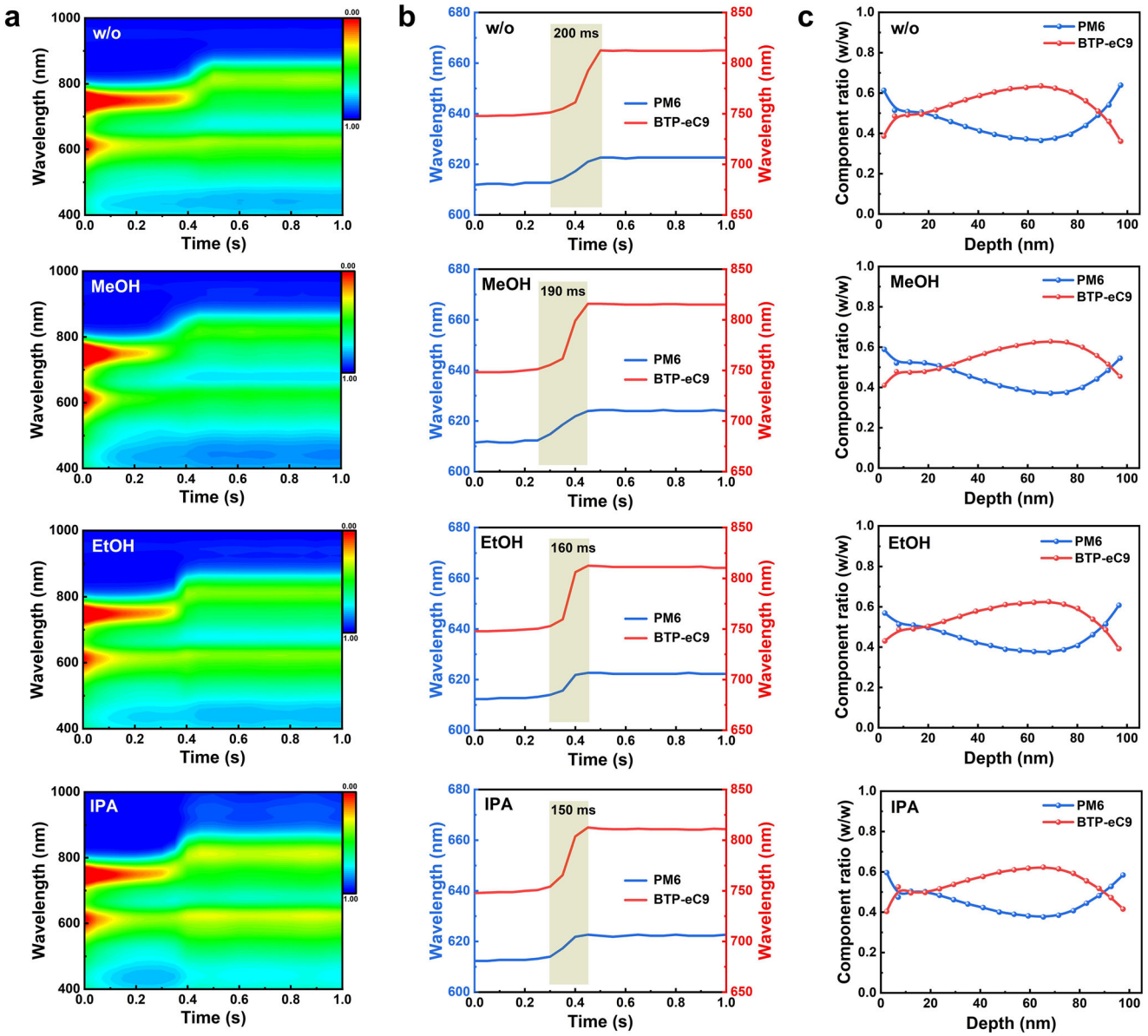


**Figure 3.** a) In situ absorption spectra, b) the maximum absorption peak location, and c) components distribution profiles of the blend films at different film-depths.

the blend films. Compared to the blend film without additives, the films with alcohol as additives show obvious decreased phase separation, which corresponds to the decreased crystallization time of BTP-eC9 in the film formation process. Notably, IPA based film exhibits a more uniform fibril-like bicontinuous network structure, which is beneficial for efficient exciton dissociation and enhanced charge transport in the devices.

To obtain deeper insights into the thin film crystallinity, grazing incidence X-ray diffraction (GIXD) measurements were performed.[32] The 2D GIXD patterns and corresponding scattering profiles in the in-plane (IP) and out-of-plane (OOP) direction are shown in Figure 4b and Figure S16 (Supporting Information). In these blend films, both the polymer donor and SMA are preferentially face-on oriented according to $\pi$–$\pi$ stacking peak locations, which facilitates carrier transport. Table S6 (Supporting Information) presents detailed information on the peak location, d-spacing, and crystal coherence length (CCL) of the (100), and (010) peaks in the blend films. As shown in Figure 4c, the (010) peaks in the OOP direction are located at 1.69, 1.76, 1.77, and 1.79 $Å^{-1}$, corresponding to d-spacing of 3.71, 3.57, 3.55, and 3.51 Å, and the CCLs deduced from the full width at half maximum (FWHM) are 25.62, 26.91, 27.14, and 32.32 Å for blend films without and with additives of MeOH, EtOH and IPA, respectively. The enhanced lamellar and $\pi$–$\pi$ stacking in the blend films indicate that the addition of IPA contributes to forming more ordered stacking (Figure 4d), which is consistent with the Urbach energy and charge carrier mobility data.

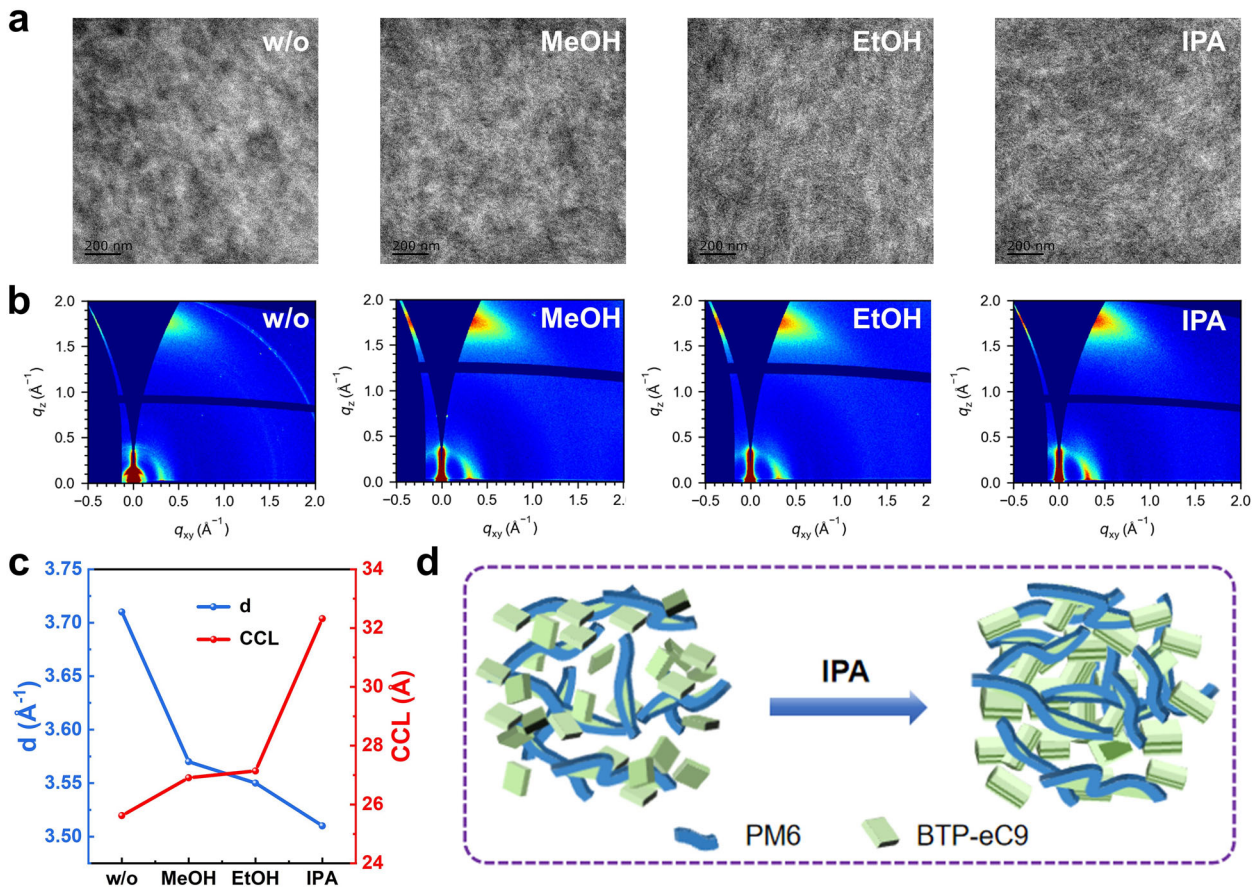


**Figure 4.** a) TEM images of the blend films. b) 2D GIXD patterns of the blend films. c) The d-spacing and CCL in the OOP direction of the blend films. d) Schematic illustration of the active layer processed with IPA as a solvent additive.

### 2.4. Universality and All-Green-Solvent-Based Devices

In order to investigate the practical application and universality of the above morphology control strategy with IPA as a solvent additive, a scalable coating method called doctor-blade coating was used to fabricate OSC devices in ambient air. An enhanced PCE of 18.2% is obtained for OSCs processed with IPA, which is mainly due to the enhanced $J_{sc}$ (Figure S17 and Table S7, Supporting Information). The inverted device with IPA as a solvent additive also exhibits improved performance compared with that of pure chloroform (Figure S18 and Table S8, Supporting Information). Furthermore, the optimal active layer solution with IPA as an additive is stable, and no precipitation occurs within 12-h storage (Figure S19a, Supporting Information). The device efficiency remains almost unchanged during the storage period (Figure S19b and Table S9, Supporting Information). These results indicate that the morphology control strategy using IPA as an additive holds significant potential for practical applications.

The universality of our morphology control strategy with IPA as an additive was further investigated by using four different other active layer systems (PM6:Y6,[33] PM6:L8-BO,[4] PM6:CH22,[34] and PM6:BO-4Cl[35]) with chloroform (CF) as the main solvent. As shown in **Figure 5a**, compared with the control device, all the IPA processed devices achieved improvements with higher PCEs, mainly attributed to the improved $J_{sc}$ and FF (Figure S20 and Table S10, Supporting Information). Then, we also fabricated all-green-solvent processed OSC devices by replacing CF with nonhalogenated solvent o-xylene. Both the PM6:BTP-eC9 and PM6:BTP-eC9-4ClO[10] based devices show enhanced $J_{sc}$ and FF with IPA as an additive, contributing to high PCEs of 19.1% and 19.4%, respectively (Figure 5b; Figure S21 and Table S11, Supporting Information). Notably, the PCE of 19.4% is among the highest values for the OSC devices processed with nonhalogenated solvents not only for the main solvents but also for the solvent additives (Figure 5c). Furthermore, PM6:BTP-eC9-4ClO based devices processed with all green solvents were also fabricated in ambient condition, and a decent PCE of 18.5% was achieved (Figure 5b; Table S11, Supporting Information). These results indicate that our morphology control strategy with IPA as a solvent additive exhibits broad applicability in OSC optimization.

## 3. Conclusion

To overcome the contradiction between the precise control of film morphology and the high toxicity of required additives, IPA is developed as a highly effective and green solvent additive for the first time. Compared to the control film, IPA processed blend film gives a more compact and ordered molecular arrangement, and optimal fiber network morphology, thus rendering the

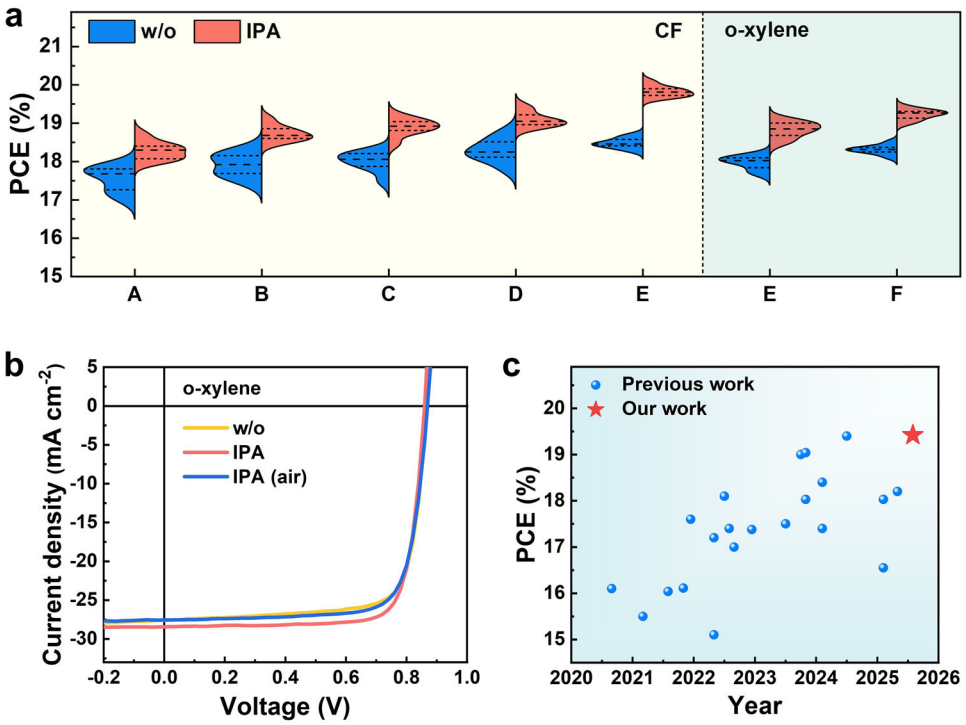


**Figure 5.** a) Violin plots of PCE distribution of OSC devices without (left) and with (right) IPA as a solvent additive. Note: A-F represent different active layers materials. (A: PM6:Y6; B: PM6:L8-BO; C: PM6:CH22; D: PM6:BO-4Cl; E: PM6:BTP-eC9; F: PM6:BTP-eC9-4ClO). b) *J-V* curves of PM6:BTP-eC9-4ClO-based OSC devices processed with o-xylene as the main solvent and different additives in the glovebox and air. c) A summary of the PCE of binary OSCs processed with all nonhalogenated solvents reported in the literature.

suppressed charge carrier recombination, more efficient exciton dissociation, and faster and balanced charge transfer processes in resulting OSCs. As a result, PM6:BTP-eC9 based device with IPA as an additive gave an impressive PCE of 20.0% with a $V_{oc}$ of 0.856 V, a $J_{sc}$ of 28.89 mA cm$^{-2}$ and an FF of 80.9%, which is much higher than the control device without additives (PCE of 18.2%). It is worth noting that an excellent PCE of 19.4% for all-green-solvent processed OSCs was also obtained, ranking among the best values for all-green-solvent systems. Furthermore, an overall investigation also demonstrated the broad applicability of IPA in various OSCs with different active layers and the benefits on long-term device stability. The morphology control strategy with IPA as a green additive may provide a new pathway to large-scale production of OSCs with high efficiency, superior stability, excellent generality, and improved eco-compatibility.

## Supporting Information

Supporting Information is available from the Wiley Online Library or from the author.

## Acknowledgements

B.G. and J.L. contributed equally to this work. The authors gratefully acknowledge the financial support from the National Key R&D Program of China (2022YFB4200400) and the National Natural Science Foundation of China (62404222, 22479081, and 22361132530).

## Conflict of Interest

The authors declare no conflict of interest.

## Data Availability Statement

The data that support the findings of this study are available from the corresponding author upon reasonable request.

## Keywords

eco-compatibility, generality, isopropanol, morphology, organic solar cells

Received: July 21, 2025
Revised: September 4, 2025
Published online: September 27, 2025

[1] G. Li, R. Zhu, Y. Yang, *Nat. Photon.* **2012**, *6*, 153.
[2] S. Günes, H. Neugebauer, N. S. Sariciftci, *Chem. Rev.* **2007**, *107*, 1324.
[3] H. Mou, Y. Yin, H. Chen, J. Xu, J. Ding, C. Ju, J. Zhu, Y. Wang, W. Chen, G. Xu, T. Zhang, J. Li, Y. Li, Y. Li, *J. Am. Chem. Soc.* **2025**, *147*, 21241.
[4] C. Li, J. Song, H. Lai, H. Zhang, R. Zhou, J. Xu, H. Huang, L. Liu, J. Gao, Y. Li, M. H. Jee, Z. Zheng, S. Liu, J. Yan, X. K. Chen, Z. Tang, C. Zhang, H. Y. Woo, F. He, F. Gao, H. Yan, Y. Sun, *Nat. Mater.* **2025**, *24*, 433.
[5] Y. Jiang, K. Liu, F. Liu, G. Ran, M. Wang, T. Zhang, R. Xu, H. Liu, W. Zhang, Z. Wei, Y. Cui, X. Lu, J. Hou, X. Zhu, *Adv. Mater.* **2025**, *37*, 2500282.

[6] J. Dong, Y. Li, C. Liao, X. Xu, L. Yu, R. Li, Q. Peng, *Energy Environ. Sci.* **2025**, *18*, 4982.
[7] L. Zhu, M. Zhang, G. Zhou, Z. Wang, W. Zhong, J. Zhuang, Z. Zhou, X. Gao, L. Kan, B. Hao, F. Han, R. Zeng, X. Xue, S. Xu, H. Jing, B. Xiao, H. Zhu, Y. Zhang, F. Liu, *Joule* **2024**, *8*, 3153.
[8] J. Xie, K. Zhang, L. Hao, Z. Yang, S. Dong, H. Li, L. Liu, J. Yu, L. Wang, J. Zhao, Y. Wang, F. Huang, *Adv. Energy Mater.* **2025**, *15*, 2501819.
[9] J. Ren, J. Wang, J. Qiao, Z. Chen, X. Hao, S. Zhang, J. Hou, *Adv. Mater.* **2025**, *37*, 2418353.
[10] R. Ma, B. Zou, Y. Hai, Y. Luo, Z. Luo, J. Wu, H. Yan, G. Li, *Adv. Mater.* **2025**, *37*, 2500861.
[11] S. Guan, Y. Li, Z. Bi, Y. Lin, Y. Fu, K. Wang, M. Wang, W. Ma, J. Xia, Z. Ma, Z. Tang, X. Lu, L. Zuo, H. Li, H. Chen, *Energy Environ. Sci.* **2025**, *18*, 313.
[12] X. Gu, Y. Wei, R. Zeng, J. Lv, Y. Hou, N. Yu, S. Tan, Z. Wang, C. Li, Z. Tang, Q. Peng, F. Liu, Y. Cai, X. Zhang, H. Huang, *Angew. Chem., Int. Ed.* **2025**, *64*, 202418926.
[13] B. Fan, H. Gao, L. Yu, R. Li, L. Wang, W. Zhong, Y. Wang, W. Jiang, H. Fu, T. Chen, B. Kan, S.-W. Tsang, A. K. Y. Jen, *Angew. Chem., Int. Ed.* **2025**, *64*, 202418439.
[14] H. Lu, D. Li, W. Liu, G. Ran, H. Wu, N. Wei, Z. Tang, Y. Liu, W. Zhang, Z. Bo, *Angew. Chem., Int. Ed.* **2024**, *63*, 202407007.
[15] Z. Chen, J. Ge, W. Song, X. Tong, H. Liu, X. Yu, J. Li, J. Shi, L. Xie, C. Han, Q. Liu, Z. Ge, *Adv. Mater.* **2024**, *36*, 2406690.
[16] F. Yang, S. R. Forrest, *ACS Nano* **2008**, *2*, 1022.
[17] Z. Wang, K. Gao, Y. Kan, M. Zhang, C. Qiu, L. Zhu, Z. Zhao, X. Peng, W. Feng, Z. Qian, X. Gu, A. K. Jen, B. Z. Tang, Y. Cao, Y. Zhang, F. Liu, *Nat. Commun.* **2021**, *12*, 332.
[18] C. Lorch, H. Frank, R. Banerjee, A. Hinderhofer, A. Gerlach, G. Li Destri, F. Schreiber, *Appl. Phys. Lett.* **2015**, *107*, 201903.
[19] L. Zhu, M. Zhang, W. Zhong, S. Leng, G. Zhou, Y. Zou, X. Su, H. Ding, P. Gu, F. Liu, Y. Zhang, *Energy Environ. Sci.* **2021**, *14*, 4341.
[20] R. S. Gurney, D. G. Lidzey, T. Wang, *Rep. Prog. Phys.* **2019**, *82*, 036601.
[21] C. McDowell, M. Abdelsamie, M. F. Toney, G. C. Bazan, *Adv. Mater.* **2018**, *30*, 1707114.
[22] D. Hu, H. Tang, C. Chen, D. J. Lee, S. Lu, G. Li, H. Y. Hsu, F. Laquai, *Adv. Mater.* **2024**, *36*, 2406949.
[23] F. Zhao, C. Wang, X. Zhan, *Adv. Energy Mater.* **2018**, *8*, 1703147.
[24] M. Kasha, H. R. Rawls, M. A. El-Bayoumi, *Pure Appl. Chem.* **1965**, *11*, 371.
[25] J. Song, C. Li, H. Ma, B. Han, Q. Wang, X. Wang, D. Wei, L. Bu, R. Yang, H. Yan, Y. Sun, *Adv. Mater.* **2024**, *36*, 2406922.
[26] V. D. Mihailetchi, J. Wildeman, P. W. Blom, *Phys. Rev. Lett.* **2005**, *94*, 126602.
[27] L. J. A. Koster, V. D. Mihailetchi, R. Ramaker, P. W. M. Blom, *Appl. Phys. Lett.* **2005**, *86*, 123509.
[28] A. Foertig, A. Baumann, D. Rauh, V. Dyakonov, C. Deibel, *Appl. Phys. Lett.* **2009**, *95*, 052104.
[29] A. A. Bakulin, A. Rao, V. G. Pavelyev, P. H. van Loosdrecht, M. S. Pshenichnikov, D. Niedzialek, J. Cornil, D. Beljonne, R. H. Friend, *Science* **2012**, *335*, 1340.
[30] A. Rao, P. C. Chow, S. Gelinas, C. W. Schlenker, C. Z. Li, H. L. Yip, A. K. Jen, D. S. Ginger, R. H. Friend, *Nature* **2013**, *500*, 435.
[31] G. Lu, Z. Shen, H. Wang, L. Bu, G. Lu, *Rev. Sci. Instrum.* **2023**, *94*, 023907.
[32] P. Muller-Buschbaum, *Adv. Mater.* **2014**, *26*, 7692.
[33] J. Yuan, Y. Zhang, L. Zhou, G. Zhang, H.-L. Yip, T.-K. Lau, X. Lu, C. Zhu, H. Peng, P. A. Johnson, M. Leclerc, Y. Cao, J. Ulanski, Y. Li, Y. Zou, *Joule* **2019**, *3*, 1140.
[34] H. Liang, X. Bi, H. Chen, T. He, Y. Lin, Y. Zhang, K. Ma, W. Feng, Z. Ma, G. Long, C. Li, B. Kan, H. Zhang, O. A. Rakitin, X. Wan, Z. Yao, Y. Chen, *Nat. Commun.* **2023**, *14*, 4707.
[35] Y. Cui, H. Yao, L. Hong, T. Zhang, Y. Tang, B. Lin, K. Xian, B. Gao, C. An, P. Bi, W. Ma, J. Hou, *Natl. Sci. Rev.* **2020**, *7*, 1239.